RSC Advances

ROYAL SOCIETY OF CHEMISTRY

www.rsc.org/advances

Graphical abstract

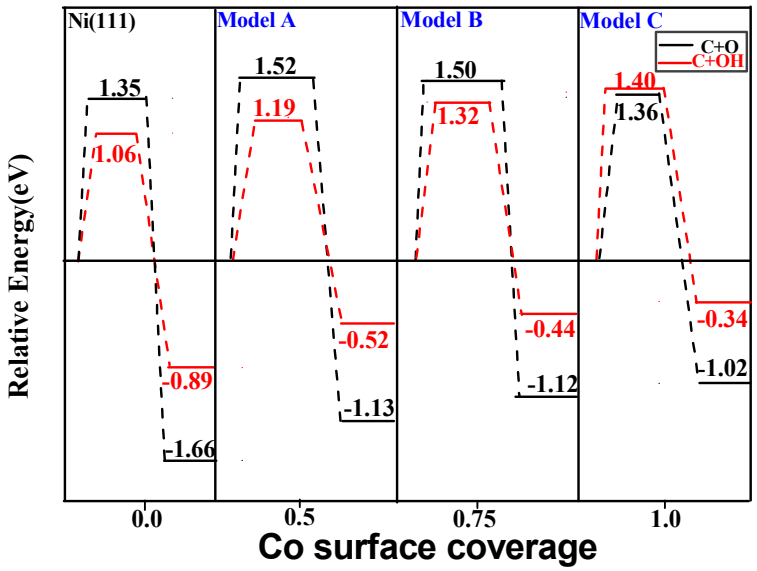

Insight into C+O(OH) Reaction for Carbon Elimination on Different types of CoNi(111) Surfaces: A DFT Study

Xiaoqiang Guo[a] *Hongyan Liu*[b] *Baojun Wang*[a,*] *Qiang Wang*[c] *Riguang Zhang*[a,*]

[a] Key Laboratory of Coal Science and Technology of Ministry of Education and Shanxi Province, Taiyuan University of Technology, Taiyuan 030024, Shanxi, P.R. China;

[b] College of Chemistry and Environment Engineering, Shanxi Datong University, Datong, Shanxi 037009, China

[c] State Key Laboratory of Coal Conversion, Institute of Coal Chemistry, Chinese Academy of Sciences, Taiyuan 030001, Shanxi, PR China

Abstract: A density-functional theory method (DFT) has been performed to investigate the reaction of C+O(OH) on three types of bimetallic alloy CoNi(111) surfaces, and the obtained results are compared with those on the pure Ni(111) surface. Our results show that the introduction of Co into Ni catalyst is beneficial for the adsorption of C, O and OH species, while it weakens the adsorption of CO. Moreover, O(OH) preferably absorbs on the CoNi(111) surfaces with the surface enrichment of Co than the homogeneous CoNi(111) surface; the increased degree of O adsorption energy overweighs the corresponding values of C on the pure Ni(111) and three types of bimetallic alloy CoNi(111) surfaces, indicating that Co has stronger affinity for oxygen species than carbon species. On the other hand, the mechanism of C+O(OH) reaction and the corresponding rate constants at different temperature show that OH species has a stronger ability of eliminating carbon than O species on Ni(111) and CoNi(111) surfaces; on CoNi(111) surface, when Co surface coverage is equal to 1 ML, compared to Ni(111), the C+O reaction can be accelerated. When Co surface coverage is equal to 3/4 ML, the C+OH reaction is the most favorable; further, the rate constants of C+OH reaction on CoNi(111) with Co surface coverage of 3/4 ML is much larger than that of C+O reaction on CoNi(111) with Co surface coverage of 1 ML. As a result, for carbon elimination on the alloy CoNi surface, OH species should serve as the key species for carbon elimination, the Co surface coverage of CoNi(111) surface should be kept 3/4 ML.

Keywords: C+O(OH) reaction; CoNi(111) surface; carbon elimination

* Corresponding author at: No. 79 Yingze West Street, Taiyuan 030024, China. Tel.: +86 351 6018239; Fax: +86 351 6041237
E-*mail address*: quantumtyut@126.com; wangbaojun@tyut.edu.cn (Baojun Wang); zhangriguang@tyut.edu.cn (Riguang Zhang)

1. Introduction

Catalytic reforming of CH_4 with CO_2 is exceptionally attractive from the view of the environmental and economical point,[1-7] since this process can provide a potential way to utilize two abundant greenhouse gases as the building block for producing synthesis gas with the ratio to unit, which is very beneficial for the synthesis processes of some liquid fuels. The supported-Ni catalyst is regarded as the most attractive catalyst for this process. However, the rapid coke accumulation on the catalyst and coke-induced deactivation are the main drawbacks to prevent its application.[8,9]

Coke accumulation on the catalyst is the result of carbon formation and carbon removal. Thus, the avoidance of coking requires the maximal rates of carbon removal and the minimization of one or more of the processes leading to carbon formation.[10] An effective way to suppress coke accumulation is to increase the feed CO_2/CH_4 ratio, and add the appropriate steam, which can result in the higher rates of carbon removal and improve the stability.[11,12] It is widely accepted that the role of CO_2 or H_2O is to provide the oxidizer of CH_x(x=1-3) species, i.e., O and OH species.[13,14] Previous studies have proposed that the oxygen intermediates, such as O and OH species, largely act as the surface cleaner to scavenge the deposited carbon, further restore the catalyst activity.[15-17] Thus, both C+O and C+OH reactions are believed to be the key step to understand carbon elimination.

A large number of studies have shown that surface O species originated from CO_2 dissociation are the key intermediate for carbon elimination, however, only a few attentions is paid to the OH species, for example, the studies by Ferreira-Aparicio *et al.*[18] have shown that surface OH species may play a key role in its resistance to deactivation by significantly decreasing the rate of carbon deposition on the metal. Meanwhile, based on the isotopic TPO experiments, Goula *et al.*[19] assumed that OH species derived from the dissociation of adsorbed H_2O can participate in the carbon removal. By means of density functional theory (DFT) calculations, Shishkin and Ziegler[20] have shown that OH species from adsorbed H_2O favorably interact with C to form CO species. According to the microkinetic analysis of the dry reforming, Maestri *et al.*[13] have reported that CH_4 consumption proceeds via the pyrolysis and carbon oxidation by the superficial OH species, which is consistent with the previous DFT slab calculations that C oxidation by OH species is more favorable than that by O species.[14,21] Above studies shows that OH species may serve as the key species for carbon elimination. Therefore, insight into the promotional effect of OH species on carbon removal is evidently needed.

Nowadays, there is much research to improve the stability and coking resistance of Ni-based catalysts. It has been suggested that the bimetallic catalysts can improve the performance of activity and stability compared to the corresponding monometallic catalysts.[22,23] In particular, Co-Ni bimetallic catalyst is proved to display the distinctive carbon-resistance ability and the excellent catalytic performance. Co has also received great attention as an active metal for the catalytic reforming of CH_4 with CO_2. Compared to Ni-based catalyst, the supported Co catalyst can exhibit a high tolerance to carbon deposition but gradually deactivated because of the oxidation,[24,25] implying that it has stronger affinity for oxygen species derived from CO_2 than carbon species. The combination of the oxygenphile nature of Co with that of Ni (stronger affinity for carbon species) is beneficial for reducing the possibility of metal oxidation and suppressing carbon formation. It is speculated that, by accelerating CH_4 decomposition, Ni provides the reductive hydrogen to Co via spillover phenomena,[26,27] which can inhibit the oxidation of the Co. Koh *et al*.[28] have found that the presence of Ni increases the reducibility of Co_3O_4 to Co, and the existence of Co leads to a decrease in the rate of coke formation by catalyzing the oxidation of surface carbon. Zhang and co-workers[29] have reported that Co-Ni bimetallic catalyst with an approximate Co/Ni ratio to one can completely eliminate carbon for up to 250 h. However, the beneficial effects of the bimetallic catalysts on carbon elimination remain unsolved, which need to be clarified.

On the other hand, the arrangement of active component and the morphology of CoNi surface is obviously affected by the reacting atmosphere, the coexistence of reductive (CH_4, H_2, CO) and oxidative (CO_2, H_2O) species. Meanwhile, Co tends to form the homogeneous structures with Ni, [30,31]or segregate on Ni surface,[29,32,33] as a result, the modification of surface morphology will in turn have an effect on the adsorption properties of key intermediates, further on the reactivity of the deposited carbon with oxygen intermediates.[25,30] However, up to now, the studies about the C+O(OH) reaction for carbon elimination on CoNi alloy is still scarce. In our previous work,[34] we have investigated the C+O reaction on the homogeneous CoNi(111) surface, but the promotional effect of OH species on carbon elimination has not been considered. More importantly, for the segregated CoNi surface, the underlying mechanisms about the reaction of carbon elimination and the effect of CoNi surface properties on carbon elimination have not been investigated.

In this study, a systematic density functional theory (DFT) study about the carbon elimination on three kinds of CoNi(111) surfaces, including the homogeneous surface, the surface with the moderate segregation of Co, and the surface with the excessive segregation of Co, has been

performed to determine the reaction mechanism of carbon elimination. The adsorption geometries and energetics involved in carbon elimination on three types of CoNi(111) surfaces are firstly discussed, then, the reactions of C+O and C+OH are investigated to elucidate the effects of Co and the structural properties of CoNi surface on the performance of carbon elimination.

2. Computational Details

2.1 Surface models

Previous studies have shown that the supported CoNi bimetallic catalysts with an approximate Ni/Co ratio to one can provide the best catalytic activity, along with the absence of coking in the reforming of CH_4 with CO_2.[29,35] According to the analysis of XRD, the formation of homogeneous alloy from bulk to surface has been observed.[31] Further, EXAFS fitting results suggested the formation of an ordered and the homogeneous fcc Co-Ni alloy with Ni≥50%.[36] Therefore, the CoNi binary system with an Ni/Co ratio to one is simulated by replacing two Ni atoms in the conventional cell of the four Ni atoms with two Co atoms. The equilibrium lattice constants of NiCo alloy are optimized to be a=3.480 Å, b=c=3.604 Å.

The surfaces are obtained by cutting alloy of NiCo along [111] direction. A rectangular ($2\sqrt{3} \times 2$) supercell with eight metal atoms at each layer is used to represent CoNi(111) surface. Meanwhile, a 12 Å vacuum slab is employed to separate the periodically repeated slabs. The first Brillouin zone of the CoNi(111) surface is sampled with a 4×4×1 k-point mesh. The bottom two layers in the slab models are constrained, and the upper two layers together with the adsorbed species are allowed to relax during all calculations. Herein, we set up the homogeneous CoNi(111) surface, which is denoted as Model A, as shown in Figure 1. However, since the reacting atmosphere has obvious effect on the structures of CoNi surface, Co is prone to segregation on the surface, as a result, another two models are constructed to represent the segregation of Co on CoNi(111) surface, one is that by exchanging two interval Ni atoms on the surface layer with two Co atoms on the subsurface layer; the other is that by exchanging four surface Ni atoms with the four Co atoms on the subsurface layer, which are called as Model B and Model C, respectively (shown in Figure 1). From Models A~C, the numbers of Co atoms presented on the surface layer are 4, 6 and 8, which corresponds to Co surface coverage of 1/2, 3/4 and 1 ML, respectively, namely, Model A represents the homogeneous surface, Model B presents the surface with the moderate segregation of Co, and Model C presents the surface with the excessive segregation of Co.

2.2 Computational methods

All DFT calculations in this study have been carried out using the Vienna *ab* initio simulation package (VASP).[37-39] The ionic cores and their interaction with the valence electrons, are described by the projector augmented wave method (PAW)[40,41] with a frozen-core approximation. The Kohn-Sham one-electron valence states are expanded in a basis of plane waves with a kinetic energy cutoff of 400 eV. The exchange-correlation energy is described with the Perdew–Burke–Ernzerhof (PBE)[42] scheme by using the generalized gradient approximation (GGA). Brillouin zone sampling is performed using a Monkhorst-Pack grid,[43] and electronic occupancies are determined according to Methfessel-Paxton scheme[44] with an energy smearing of 0.1 eV. Since two magnetic elements of Ni and Co are involved in the system, the spin-polarized effect has been considered. The relaxation of the electronic degrees of freedom is assumed to be converged if the total energy change and the band structure energy change between two steps are both smaller than 10^{-6} eV/Å. A force difference between two steps less than 0.01 eV/Å is used as the criterion for convergence of relaxation. Our calculated lattice constant of Ni (3.518 Å) agrees with the previous theoretical values (3.522 Å)[45] and the experimental value (3.52 Å).[46]

Reaction paths have been investigated using the climbing-image nudged elastic band method (CI-NEB).[47,48] Transition states have been optimized using the dimer method.[49,50] The transition state structure is thought to be converged when the forces acting on the atoms are all less than 0.05 eV/Å for the various degrees of freedom set in the calculation.

The adsorption energy, E_{ads}, is defined as follows:

$$E_{ads} = E_{(adsorbate/slab)} - E_{slab} - E_{adorbate}$$

where $E_{adsorbate/slab}$ is the total energies of adsorbate on the slab model, E_{slab} is the total energy of the clean slab model. $E_{adsorbate}$ is the total energy of the isolated adsorbate obtained in a 10×10×10 Å cubic cell.

3. Results and Discussion

3.1 Adsorption of reaction intermediates

In order to obtain the most stable adsorption configurations of related species involved in carbon elimination, various adsorption sites on the pure Ni(111) and the alloyed CoNi surfaces have been considered. There are four sites on the pure Ni(111) surface: Top (T), Bridge (B), Hexagonal-close-packed (Hcp) and Face-centered-cubic (Fcc). On the alloyed CoNi(111) surface,

several new adsorption sites are formed due to the existence of two constituents in the lattice. According to the previous calculations on Ni(111),[14,21,51] the intermediates related to carbon elimination prefer to absorb at the Fcc and Hcp sites. Therefore, the threefold hollow sites of the alloyed CoNi surface are considered and highlighted in Figure 1. Figure 2 presents the stable adsorption configurations of the related species involved in carbon elimination on Ni(111) surface. Our calculated adsorption sites for different adsorbates on Ni(111) are in good agreement with the previously reported values.[14, 21] The calculated adsorption energies for all possible species at the threefold hollow sites on three types of CoNi(111) surface models are summarized in Table 1, and the corresponding adsorption structures are shown in Figures 3~5, respectively.

3.1.1 C adsorption

Our results show that the initial configurations of C atom adsorbed at the bridge and top site on Ni(111) surface are optimized into that at the threefold site after geometry optimization. On CoNi(111) surface, the most favorable site on Model A is Hcp1 site, while it is Hcp3 site on Model B, and Hcp site on Model C. The adsorption energy on Model C is -7.12 eV, it is slightly more negative by 0.06 eV than that on Model B, and by 0.14 and 0.24 eV than those on Model A and Ni(111) surface, respectively, indicating that the introduction of Co leads to the increase of C adsorption stability compared to the pure Ni(111) surface.

3.1.2 O adsorption

Similar to C adsorption on Ni(111), O atom located at the top site and bridge sites is inclined to transfer to the threefold site after geometry optimization. The most stable site for O species on Ni(111) is found to be Fcc site with an adsorption energy of -5.76 eV, which is more stable by 0.12 eV than that at the Hcp site. On CoNi(111), the most favorable O adsorption site on Models A~C is similar to the case of C atom adsorption on CoNi(111). We can see from Table 1 that the adsorption energy of the most stable adsorbed O increases from -5.76 eV on Ni(111), to -5.99 eV on Model A, to -6.12 eV on Model B, to -6.86 eV on Model C. Clearly, the introduction of Co significantly promotes the adsorption stability of O species.

On the other hand, O absorbed on Models B and C with the surface enrichment of Co is more favorable than that on Model A, and the increased degree of O adsorption energy far outstrips the corresponding values of C atom adsorption on Ni(111) and Models A~C, indicating that Co has stronger affinity for oxygen species than carbon species. The stability order for all configurations on Model A is as follows: Hcp1≈Fcc1>Fcc2≈Hcp2, that on Model B is Hcp3≈Fcc3>Fcc4≈Fcc1≈

Hcp1>Hcp4, and that on Model C is Hcp>Fcc1≈Fcc2.

3.1.3 OH adsorption

OH is preferably absorbed at the threefold site with the O-H bond oriented perpendicular to the Ni(111) and three types of CoNi(111) surfaces. On Ni(111), OH binding at the Fcc site is more favored than that at the Hcp site. On Model A, four stable structures are verified; the most favorable adsorption site is Fcc1 site with an adsorption energy of -3.68 eV. Other three adsorption energies are -3.64 eV at the Hcp1, -3.42 eV at the Hcp2, and -3.44 eV at the Fcc2, respectively. On Model B, there are six stable configurations at the threefold site, Hcp3 and Fcc3 sites surrounded by three Co atoms are the most stable adsorption site with the equal adsorption energy of -3.79 eV, which is energetically more favorable than that on Model A. On Model C, OH binding at the Fcc1 site with the adsorption energy of -3.78 eV is slightly favored than those at the Hcp and Fcc2 sites. Our results indicate that the segregation of Co is beneficial for OH adsorption. Moreover, it is noteworthy that the adsorption energies become more negative on the alloyed CoNi(111) surface compared to that on the pure Ni(111). Thus, the introduction of Co still enhance the adsorption ability of OH species.

3.1.4 COH adsorption

It is found that the initial adsorption configurations of COH at the top and bridge site are unstable, and COH putted initially at these two sites are all relaxed to the threefold site after geometry optimization. From Table 1, we can see that the adsorption energies of COH binding at the threefold site on Ni(111), Model B and C are rather close (the energy difference is only within 0.06 eV), respectively, suggesting that there is no obvious site-preference. However, on Model A, the most favorable COH adsorption site is Hcp1 site, where C atom is located at the center of the site, and the C-O bond is parallel to the surface normal. Further, the differences of adsorption energies are very small on Ni(111) and Models A~C (-4.39, -4.35, -4.43 and -4.49 eV, respectively), indicating that the introduction of Co has few effect on the adsorption stability of COH species.

3.1.5 CO adsorption

CO adsorption on the alloyed CoNi(111) and Ni(111) surfaces is different from the species mentioned above. CO located at the top site and bridge site can exist. On Ni(111) surface, four stable adsorption configurations are obtained, the corresponding adsorption energies are -1.89 eV at the Hcp site, -1.87 eV at the Fcc site, -1.76 eV at the Bridge site, and -1.53 eV at the Top site, respectively, which clearly show the order of adsorption energy: Hcp≈Fcc>Bridge>Top. On CoNi(111), there are seven stable configurations on Model A, eight stable configurations are verified

on Model B, and four stable configurations are confirmed on Model C. CO binding at the Ni-Co bridge site on Model A exits, CO located at other bridge sites on Models A~C tend to transfer to the stable threefold site after geometry optimization. On Models B, C and Ni(111), CO binding at the threefold site is more preferred than those at the top and bridge sites, while for CO absorbed at the Ni-Co bridge site and Co top site on Model A, the adsorption energies differences are very small. Compared to Ni(111), it can be deduced that the introduction of Co into Ni catalyst weakens the adsorption ability of CO, which agrees with the previous results obtained by the experimental observations [31,35] and the theoretical calculations.[34]

3.2 Mechanism for Carbon Elimination Reactions of C+O and C+OH

3.2.1 Carbon elimination on Ni(111)

Figure 6 presents the configurations of the initial states (IS), transition states (TS), and final states (FS) for carbon elimination reactions of C+O and C+OH on Ni(111). C preferably absorbs at the Hcp and Fcc site due to the small difference of adsorption energy, and O(OH) favorably binds at the Fcc site. Two stable co-adsorption structures of C and O(OH) are obtained, and chosen as the initial states; In the final states, since the differences of adsorption energy for CO(COH) species is very small between Hcp and Fcc site, CO(COH) species is located at the Hcp or Fcc site according to the corresponding IS configuration. The activation barriers and reaction energies for C+O and C+OH reactions are listed in Table 2.

(A) C+O Reaction

As shown in Figure 6, Path 1 is that the co-adsorbed C and O, which is absorbed at the Hcp and Fcc site, respectively, combines to form CO via TS1 along with O moving through the top of Ni, and the C-O distance is shortened from 3.21 Å in IS to 1.87 Å in TS1, and 1.19 Å in FS. This step is exothermic by 1.50 eV, and needs to overcome a high activation barrier of 2.29 eV. In Path 2, the co-adsorbed configuration of C and O atoms at two Fcc sites in a zigzag way is chosen as the initial state, and CO binding at the Hcp site is chosen as the final state; in TS2, O atom transfers to the Ni-Ni bridge site, C atom absorbed at its original site; the activation barrier of Path 2 via TS2 is 1.35 eV with the reaction energy of -1.66 eV, which are lower than that of Path 1, namely, Path 2 is more favorable both thermodynamically and kinetically than Path 1.

(B) C+OH Reaction

Similarly, two paths are considered for C+OH reaction. In Path 1, C adsorbed at the Hcp site associates with OH at the Fcc site to form COH via TS3; in TS3, OH is located at the top of Co, C

resides its original site, and the C-O bond length is shortened from 3.22 Å in IS to 2.13 Å in TS3; this reaction is exothermic by 0.74 eV with the activation barrier of 1.26 eV. Path 2 involves that C and OH co-adsorb at two Fcc sites in a zigzag way, which can couple to form COH via TS4; in TS4, C adsorbed at the Fcc site, OH interacts with a Ni atom to approach the Hcp site. This reaction needs to overcome a low activation barrier of 1.06 eV with the reaction energy of -0.89 eV, which are lower than those of Path 1, namely, Path 2 is more favorable both thermodynamically and kinetically than Path 1.

Above results show that Path 2 is the most favorable pathway for C+O and C+OH reactions. The activation barrier of C+OH reaction is lower by 0.29 eV than that of C+O reaction, which means that OH species is more favorable for carbon elimination than O species.

On the other hand, our calculated activation barriers of the most favorable path for C+O and C+OH reactions on a $p((2\sqrt{3} \times 2))$ Ni(111) surface are 1.35 eV and 1.06 eV, respectively, which are in agreement with the previous calculation values (1.33 eV and 1.20 eV)[21] with a $p(3\times3)$ Ni(111) surface. Meanwhile, the discrepancies for the activation barriers of the C+O(OH) reaction exist due to the use of the different size Ni(111) surface, for example, Wang and his co-workers[52] obtained an activation barrier of 0.64 eV for the C+O reaction on a three-layer $p(2\times2)$ model using DFT calculations. Liu *et al*.[34] used the similar model and methods, and obtained a larger activation barrier (E_a=0.86 eV) for the C+O reaction. In other work, Zhu *et al*.[14] reported that the activation barrier of the C+O(OH) reaction is 1.59 eV (1.46 eV) using a periodic four-layer $p(3\times3)$ slab model, and both are reduced to 1.43 eV (1.34 eV) with the zero-point energy correction. Above studies suggested that the selected size of the model significantly affect the activation barriers of the C+O(OH) reaction. Moreover, there are the large repulsive interactions between C and O(OH) in the co-adsorption configuration on a $p(2\times2)$ model, for example, the lateral interaction energies of C and O in the linear and zigzag way are 0.58 and 1.01 eV, respectively. In contrast, for the same co-adsorption modes of C and O in our study, the lateral interaction energies are much lower (0.14 and 0.33 eV, respectively). Therefore, to avoid the uncertainty induced from the lateral interaction, we focus on our results calculated by using a $p(2\sqrt{3} \times 2)$ model.

3.2.2 Carbon elimination on Model A of CoNi(111)

Our result show that on the homogeneous alloy CoNi surface, Model A, the most favorable adsorption site of C is Hcp1 site, O(OH) species prefer to be absorbed at the Hcp1 and Fcc1 sites due

to relatively small energy difference of adsorption energy. Two co-adsorption configurations of C and O(OH) are found, and selected as the initial states. The final states consist of CO adsorbed at the T-Co, B-Ni-Co and Hcp1 site (The energy difference is within 0.04 eV), and COH located at the Hcp1 site according to the corresponding IS configuration. The geometries and parameters of all possible transition states along the reaction of carbon elimination are presented in Figures 7 and 8, respectively.

(A) C+O Reaction

For C+O reaction, six possible paths are mapped out. In Path 1, the co-adsorption of C and O sharing one Co atom in a zigzag way resides at the Hcp1 site, and couples to produce CO adsorbed at the Hcp1 site via TS A1, in which C is located at its original site, and O transfers to the Ni-Co bridge site; the corresponding activation barrier and reaction energy are 1.52 and -1.13 eV, respectively. Path 2 is that C and O co-adsorb at the Hcp1 and Fcc1 sites, respectively, both react each other to form CO via TS A2; in TS A2, the distance of C-O is shortened to 1.85 Å from 3.06 Å; this step is an exothermic process by 0.94 eV with the activation barrier of 1.61 eV. In Paths 3-6, the initial states of Paths 3 and 5 resemble that in Path 1, while those in Paths 4 and 6 are similar to that in Path 2. The final states of Paths 3 and 4 consist of CO adsorbed at the T-Co site, whereas Paths 5 and 6 take CO adsorbed at the Ni-Co bridge site as the final states. Four paths involve a similar transition state, whose geometry resembles those in Paths 1 and 2. The reaction barriers in the Paths 3 and 5 are approximately equal, which are more favorable kinetically compared to Paths 4 and 6. Meanwhile, all reaction paths are exothermic, namely, they are favorable in thermodynamic. In dynamics, Paths 1, 3 and 5 has the lowest reaction barrier among the six possible paths. Considering the reaction kinetics and thermodynamics, Path 1 is thought to be the most favorable path for C+O reaction to form CO on Model A.

(B) C+OH Reaction

Two possible paths are conceived for C+OH reaction. The co-adsorbed structure of C+OH is similar to the co-adsorption of C+O in Paths 1 and 2. The final states consist of COH adsorbed at the Hcp1 site. In Paths 1~2, C associates with OH into COH via a similar transition state, in which OH transfers to the top of Co, and C is located at its original site. Our results show that Path 1 is more favorable kinetically than Path 2. Path 1 is exothermic by 0.52 eV with an activation barrier of 1.19 eV, which is lower than that of the most favorable path (1.52 eV) for C+O reaction. Obviously, OH species is more preferred for carbon elimination than O species on the homogeneous CoNi surface.

3.2.3 Carbon elimination on Model B of CoNi(111)

On Model B, C atom prefers to absorb at the Hcp3 and Hcp1 site, O(OH) binding at the Hcp3 and Fcc3 site is more favorable, as a result, two stable co-adsorption structures of C and O(OH) are obtained, which are considered as the initial states of carbon elimination. The final states consist of CO and COH adsorbed at the Hcp1 and Hcp3 site, respectively. The structures of the stationary states for the reaction of carbon elimination on Model B are displayed in Figure 9.

(A) C+O Reaction

Two possible paths are designed for C+O reaction. In Path 1, C and O co-adsorb at the Hcp1 site and Hcp3 site, respectively, both can react to form CO adsorbed at the Hcp1 site via TS B1. In TS B1, O moves to the Co-Co bridge site, C leaves its original site, the distance of C-O is shortened to 1.80 Å in TS, and the forming C-O bond in FS is 1.20 Å; this reaction is exothermic by 1.04 eV with an activation barrier of 1.50 eV. In Path 2, the co-adsorption of C and O absorbed at the Hcp3 and Fcc3 sites can react to form CO absorbed at the Hcp3 site via TS B3; this reaction is exothermic by 0.77 eV with an activation barrier of 1.72 eV, which is higher by 0.22 eV than that in Path 1. As a result, considering the reaction kinetics and thermodynamics, Path 1 is the most favorable both kinetically and thermodynamically than Path 2.

(B) C+OH Reaction

Similarly, two possible paths are conceived for C+OH reaction. As displayed in Figure 9, the co-adsorption structures of C+OH are similar to corresponding structures of C+O, COH is located at the Hcp1 and Hcp3 sites, respectively. Two paths involve a similar transition state, which resembles TS A5 on Model A. As listed in Table 2, Path 1 is the most favorable reaction path both thermodynamically and kinetically than Path 2. Path 1 is exothermic by 0.44 eV with activation barrier of 1.32 eV, which is lower by 0.18 eV than that of the most favorable path for C+O reaction. Therefore, OH species has a stronger ability to eliminate carbon deposition than O species on the CoNi alloy with the surface enrichment of Co.

3.2.4 Carbon elimination on Model C of CoNi(111)

The geometries of the ISs, TSs, and FSs for C+O and C+OH reactions on Model C are presented in Figure 10. The activation barriers and reaction energies are also listed in Table 2.

(A) C+O Reaction

The co-adsorbed C and O binding at two Hcp sites in a zigzag way is chosen as the IS, CO located at the Hcp site is chosen as the FS. The obtained TS configuration is similar to TS B2 on

Model B, in which C is located at the Hcp site, and O is positioned at the adjacent Co-Co bridge site. This reaction is exothermic by 1.02 eV with an activation barrier of 1.36 eV.

(B) C+OH Reaction

Three possible paths are conceived for C+OH reaction since OH positioned at the Fcc1, Hcp and Fcc2 sites have the equal adsorption stability. Our results show that Path 2 is the most favorable reaction both thermodynamically and kinetically compared to Paths 1 and 3. Path 2 is exothermic by 0.34 eV with an activation barrier of 1.40 eV, which is larger than that of C+O reaction, indicating that both O species have the relatively strong ability to remove carbon deposition on Model C with the excessive segregation of Co.

3.3. Brief summary for the mechanism of C+O(OH) reaction

In order to elucidate the effect of different active component surfaces on carbon elimination, we compare the C+O and C+OH reactions on the alloyed CoNi(111) and the pure Ni(111) surfaces. The activation barrier and reaction energy for the most favorable path of C+O and C+OH reactions on these different surfaces is also displayed in Table 2.

For the reaction of C+O→CO, on Ni(111) surface, the most favorable path needs to overcome an activation barrier of 1.35 eV, which is lower than those on Models A and B by 0.17 and 0.15 eV, respectively, namely, when Co surface coverage of CoNi(111) surface is equal to 1/2 and 3/4 ML, the C+O reaction is obviously restrained. Meanwhile, the activation barrier of C+O reaction on Model A is approximately equal to that on Model B, indicating that the moderate segregation of Co on the alloy CoNi(111) surface from 1/2 to 3/4 ML has few effect on C+O reaction. However, the activation barrier of the most favorable path on Model C with the excessive segregation of Co is 1.36 eV, which is lower than those on Models A and B, suggesting that when Co surface coverage of CoNi(111) surface is equal to 1 ML, the C+O reaction is accelerated on the alloy CoNi(111) surface. For the reaction of C+OH→COH, the activation barrier (1.06 eV) of the most favorable path on Ni(111) is less than those on Models A~C (1.19, 1.32 and 1.40 eV, respectively), suggesting that as Co segregation increases, the C+OH reaction is obviously restrained. Further, our results show that compared to Ni(111) surface, the reaction energy of C+O(OH) increases with the increasing of Co surface coverage of the alloy CoNi(111) surface, namely, the exothermic energy decreases.

On the other hand, we can see from Table 2 that the activation barrier of the C+OH reaction is much lower than those of the C+O reaction on Ni(111), Models A and B, respectively, namely, when Co surface coverage is less than and equal to 3/4 ML, OH species has a stronger ability of

eliminating carbon than O species. When Co surface coverage of CoNi(111) surface increase to 1 ML, O species is slightly favorable for carbon elimination than OH species. Meanwhile, our results on CoNi(111) surface show that the activation barrier of C+O reaction on Model C with Co surface coverage of 1 ML is much larger than that of C+OH reaction on Model A with Co surface coverage of 1/2 ML. Therefore, for carbon elimination on the alloy CoNi surface, OH species should serve as the key species for carbon elimination rather than O species, the Co surface coverage of CoNi(111) surface should be kept 1/2 ML.

3.4. Effect of temperature on C+O and C+OH reactions

Previous studies have reported that catalytic reforming of CH_4 with CO_2 is a highly endothermic reaction, which requires the operating temperatures of 800~1000 K to obtain the high equilibrium conversion of CH_4 and CO_2 to H_2 and CO, and to minimize the thermodynamic driving force for carbon deposition.[53] Therefore, to further understand the effect of temperature on the reactions of C+O(OH) on Ni(111) and the alloyed CoNi(111) surfaces, we have calculated the rate constants of the most favorable path of C+O(OH) reaction at the temperature of 800, 850, 900, 950 and 1000 K, respectively, the corresponding results are listed in Table 3. The detailed description for the rate constant calculation has been given out in the Supporting Information.

From Table 3, we can see that the rate constant *k* of C+O(OH) reaction increases rapidly with the temperature increasing on Ni(111) and the alloyed CoNi(111) surfaces; at the same temperature, the rate constant of C+OH reaction is larger than that of C+O reaction on the same catalyst surface, indicating that OH species has a stronger ability of eliminating carbon than O species. For C+O reaction, at the same temperature, the rate constant is in the order of Model C>Ni(111)>Model B>Model A, which shows that the C+O reaction is obviously restrained on Models A~B, however, compared to Ni(111) surface, the C+O reaction is accelerated on Model C. namely, when Co surface coverage reaches to 1 ML, the ability of carbon elimination of C+O reaction on the alloy CoNi surface is more favorable than that on Ni(111) surface. For C+OH reaction, the rate constant is in the order of Ni(111)>Model B>Model A>Model C at the same temperature, which means that compared to Ni(111), the C+OH reaction is obviously restrained on Models A~C; further, the rate constants of C+OH reaction on Model B is much larger than that of C+O reaction on Model C.

As a result, for carbon elimination on the alloy CoNi surface, OH species should serve as the key species for carbon elimination, the Co surface coverage of CoNi(111) surface should be kept 3/4 ML, which is different from the results obtained by activation barrier. The discrepancies may be due

to that the activation barrier is calculated under the temperature of 0 K, but the rate constants are calculated under the temperature of 800~1000 K, indicating that reaction temperature obviously affects the kinetic of C+O(OH) reaction under the realistic condition.

4. Conclusions

In this work, we have carried out a systematic DFT study to investigate the adsorption of C, OH, O, COH and CO species involved in carbon elimination, as well as the mechanism of C+O(OH) reaction on three types of the alloyed CoNi(111) surface and the pure Ni(111) surface. For the alloyed CoNi(111) surface, three models, the homogeneous surface (Model A), the surface with moderate segregation of Co (Model B), the surface with excessive segregation of Co (Model C), have been constructed to represent CoNi(111) surface with the different surface Co segregation. Our results show that compared to the pure Ni(111), the incorporation of Co into Ni catalyst increase the adsorption stability of C, O and OH species, but weakens the adsorption stability of CO species, and has few effect on COH adsorption. Meanwhile, Co has stronger affinity for oxygen species than carbon species. On the other hand, the mechanism and rate constants of C+O(OH) reaction shows that OH species is more favorable for carbon elimination than O species on Ni(111) and the alloy CoNi(111) surfaces; on the alloy CoNi(111) surface, when Co surface coverage is equal to 1 ML, compared to Ni(111), the C+O reaction can be accelerated. For the C+OH reaction, on CoNi(111) surface, when Co surface coverage is equal to 3/4 ML. the C+OH is obviously favorable according to the rate constant calculations. Further, the rate constants of C+OH reaction on CoNi(111) with Co surface coverage of 3/4 ML is much larger than that of C+O reaction on CoNi(111) with Co surface coverage of 1 ML, suggesting that OH species should serve as the key species for carbon elimination on the alloy CoNi surface, the Co surface coverage of CoNi(111) surface should be kept at 3/4 ML for carbon elimination on the alloy CoNi surface.

ACKNOWLEDGMENT

This work is financially supported by the National Natural Science Foundation of China (No. 21276171, 21276003 and 21476155), the Natural Science Foundation of Shanxi Province (No. 2014011012-2) and the Top Young Innovative Talents of Shanxi.

References

(1) Fan, M. S.; Abdullah, A. Z.; Bhatia. S. Catalytic Technology for Carbon Dioxide Reforming of Methane to Synthesis Gas. *ChemCatChem* **2009**, *1*, 192−208.

(2) Bradford, M. C. J.; Vannice, M. A. CO_2 Reforming of CH_4. *Catal. Rev*. **1999**, *41*, 1−42.

(3) Ginsburg, J. M.; Piña, J.; Solhet, T. El.; Lasa, H. I. Coke Formation over a Nickel Catalyst under Methane Dry Reforming Conditions: Thermodynamic and Kinetic Models. *Ind. Eng. Chem. Res.* **2005**, *44*, 4846−4854.

(4) Tomishige, K.; Chen, Y. G.; Yokoyama, K.; Fujimoto, K. Catalytic Performance and Catalyst Structure of Nickel–Magnesia Catalysts for CO_2 Reforming of Methane. *J. Catal*. **1999**, *184*, 479−490.

(5) Cheng, D.; Zhu, X.; Ben, Y. Carbon Dioxide Reforming of Methane over Ni/Al_2O_3 Treated with Glow Discharge Plasma. *Catal. Today* **2006**, *115*, 205−210.

(6) Tang, S.; Ji, L.; Lin, J.; Zeng, H. C.; Tan, K. L.; Li, K. CO_2 Reforming of Methane to Synthesis Gas over Sol–Gel-made $Ni/\gamma\text{-}Al_2O_3$ Catalysts from Organometallic Precursors. *J. Catal*. **2000**, *194*, 424−430.

(7) Kim, J. H.; Suh, D. J.; Park, T. J.; Kim, K. L. Effect of Metal Particle Size on Coking during CO_2 Reforming of CH_4 over Ni–Alumina Aerogel Catalysts. *Appl. Catal. A: Gen.* **2000**, *197*, 191−200.

(8) Zhang, J.; Wang, H.; Dalai, A. K. Effects of Metal Content on Activity and Stability of Ni-Co Bimetallic Catalysts for CO_2 Reforming of CH_4. *Appl. Catal. A: Gen*. **2008**, *339*, 121−129.

(9) Vasileiadis, S.; Ziaka-Vasileiadou, Z. Biomass Reforming Process for Integrated Solid Oxide-Fuel Cell Power Generation. *Chem. Eng. Sci*. **2004**, *59*, 4853−4859.

(10) Trimm, D. L. Coke Formation and Minimisation during Steam Reforming Reactions. *Catal. Today* **1997**, *37*, 233−238.

(11) Rezaei, M.; Alavi, S. M.; Sahebdelfar, S.; Yan, Z, F. Nanocrystalline Zirconia as Support for Nickel Catalyst in Methane Reforming with CO_2. *Energy Fuel* **2006**, *20*, 923−929.

(12) Li, Y.; Wang, Y.; Zhang, X.; Mi, Z. Thermodynamic Analysis of Autothermal Steam and CO_2 Reforming of Methane. *Int. J. Hydrogen Energy* **2008**, *33*, 2507−2514.

(13) Maestri, M.; Vlachos, D. G.; Beretta, A.; Gropp, G. Steam and Dry Reforming of Methane on Rh: Microkinetic Analysis and Hierarchy of Kinetic Models. *J. Catal*. **2008**, *259*, 211−222.

(14) Zhu, Y. A.; Chen, D.; Zhou, X. G.; Yuan, W. K. DFT Studies of Dry Reforming of Methane on

Ni Catalyst. *Catal. Today* **2009**,*148*, 260−267.

(15) Solymosi, F.; Tolmacsov, P.; Zaka, T. S. Dry Reforming of Propane over Supported Re Catalyst. *J. Catal*. **2005**, *233*, 51−59.

(16) Siahvashi, A.; Adesina, A. A. Kinetic Study of Propane CO_2 Reforming over Bimetallic Mo–Ni/Al_2O_3 Catalyst. *Ind. Eng. Chem. Res*. **2013**, *52*, 15377−15386.

(17) Sutton, D.; Moisan, J. F.; Ross, J. R. H. Kinetic Study of CO_2 Reforming of Propane over Ru/Al_2O_3. *Catal. Lett*. **2001**, *75*, 175−181.

(18) Ferreira-Aparicio, P.; Rodrıguez-Ramos, I.; Anderson, J. A.; Guerrero-Ruiz, A. Mechanistic Aspects of the Dry Reforming of Methane over Ruthenium Catalysts. *Appl. Catal. A: Gen.* **2000**, *202*, 183−196.

(19) Goula, M. A.; Lemonidou, A. A.; Efstathiouy, A. M. Characterization of Carbonaceous Species Formed during Reforming of CH_4 with CO_2 over Ni/CaO-Al_2O_3 Catalysts Studied by Various Transient Techniques. *J. Catal*. **1996**, *161*, 626−640.

(20) Shishkin, M.; Ziegler, T. Coke-Tolerant Ni/$BaCe_{1-x}Y_xO_{3-\delta}$ Anodes for Solid Oxide Fuel Cells: DFT+U Study. *J. Phys. Chem. C* **2013**, *117*, 7086−7096

(21) Wang, S. G.; Cao, D. B.; Li, Y. W.; Wang, J.; Jiao, H. Reactivity of Surface OH in CH_4 Reforming Reactions on Ni(111): A Density Functional Theory Calculation. *Surf. Sci*. **2009**, *603*, 2600−2606.

(22) Hou, Z.; Yashima, T. Small Amounts of Rh-Promoted Ni Catalysts for Methane Reforming with CO_2. *Catal. Lett*. **2003**, *89*, 193−197.

(23) Li, X.; Ai, J.; Li, W.; Li, D. Ni-Co Bimetallic Catalyst for CH_4 Reforming with CO_2. *Front. Chem. Eng. China* **2010**, *4*, 476−480.

(24) Nagaoka, K.; Takanabe, K.; Aika, K. Modification of Co/TiO_2 for Dry Reforming of Methane at 2MPa by Pt, Ru or Ni. *Appl. Catal. A: Gen*. **2004**, *268*, 151−158.

(25) San-José-Alonso, D.; Juan-Juan, J.; Illán-Gómez, M. J.; Román-Martínez, M. C. Ni, Co and Bimetallic Ni–Co Catalysts for the Dry Reforming of Methane. *Appl. Catal. A: Gen*. **2009**, *371*, 54−59.

(26) Conner Jr, W. C.; Pajonk, G. M.; Teichner, S. J. Spillover of Sorbed Species. *Adv. Catal*. **1986**, *34*, 1−79.

(27) Conner Jr, W. C.; Falconer, J. L. Spillover in Heterogeneous Catalysis. *Chem. Rev*. **1995**, *95*, 759−788.

(28) Koh, A. C. W.; Chen, L.; Leong, Kee. W.; Johnson, B. F. G. Hydrogen or Synthesis Gas Production via the Partial Oxidation of Methane over Supported Nickel–Cobalt Catalysts. *Int. J. Hydrogen Energy* **2007**, *32*, 725−730.

(29) Zhang, J.; Wang, H.; Dalai, A. K. Development of Stable Bimetallic Catalysts for Carbon Dioxide Reforming of Methane. *J. Catal*. **2007**, *249*, 300−310.

(30) Chen, L.; Zhu, Q.; Wu, R. Effect of Co–Ni Ratio on the Activity and Stability of Co–Ni Bimetallic Aerogel Catalyst for Methane Oxy-CO_2 Reforming. *Int. J. Hydrogen Energy* **2011**, *36*, 2128−2136.

(31) Takanabe, K.; Nagaoka, K.; Nariai, K. Titania-Supported Cobalt and Nickel Bimetallic Catalysts for Carbon Dioxide Reforming of Methane. *J. Catal*. **2005**, *232*, 268−275.

(32) Djinović, P.; Črnivec, I. G. O.; Erjavec, B.; Pintar, A. Details Behind the Self-Regeneration of Supported NiCo/$Ce_{0.8}Zr_{0.2}O_2$ Bimetallic Catalyst in the CH_4-CO_2 Reforming Reaction. Chem CatChem **2014**, DOI: 10.1002/cctc.201400059.

(33) Xu, J.; Zhou, W.; Li, Z.; Wang, J.; Ma, J. Biogas Reforming for Hydrogen Production over Nickel and Cobalt Bimetallic Catalysts. *Int. J. Hydrogen Energy* **2009**, *34*, 6646−6654.

(34) Liu, H.; Zhang, R.; Ding, F.; Yan, R.; Wang, B.; Xie, K. A First-Principles Study of C+O Reaction on NiCo(111) Surface. *Appl. Surf. Sci*. **2011**, *257*, 9455−9460.

(35) Takanabe, K.; Nagaoka, K.; Nariai, K. Improved Resistance Against Coke Deposition of Titania Supported Cobalt and Nickel Bimetallic Catalysts for Carbon Dioxide Reforming of Methane. *Catal. Lett*. **2005**, *102*, 153−157.

(36) Zhang, H.; Yao, T.; Sun, Z.; Li, Y.; Liu, Q.; Hu, F. Structural Study on Co-Ni Bimetallic Nanoparticles by X-ray Spectroscopy. *J. Phys. Chem. C* **2010**, *114*, 13596−13600.

(37) Kresse, G.; Furthmüller, J. Efficient Iterative Schemes for Ab Initio Total-Energy Calculations Using a Plane-Wave Basis Set. *Phys. Rev. B* **1996**, *54*, 11169−11186.

(38) Kresse, G.; Furthmüller, J. Efficiency of Ab-Initio Total Energy Calculations for Metals and Semiconductors Using a Plane-Wave Basis Set. *Comp. Mater. Sci*. **1996**, *6*, 15−50

(39) Kresse, G.; Hafner, J. Ab Initio Molecular Dynamics for Open-Shell Transition Metals. *Phys. Rev. B*. **1993**, *48*, 13115−13118.

(40) White, J. A.; Bird, D. M. Implementation of Gradient-Corrected Exchange-Correlation Potentials in Car-Parrinello Total-Energy Calculations. *Phys. Rev. B* **1994**, *50*, 4954−4957

(41) Blochl, P. E. Projector Augmented-Wave Method. *Phys. Rev. B*. **1994**, *50*, 17953−17979.

(42) Perdew, J. P.; Burke, K.; Ernzerhof, M. Generalized Gradient Approximation Made Simple. *Phys. Rev. Lett.* **1996**, *77*, 3865−3868.

(43) Chadi, D. J. Special Points for Brillouin-Zone Integrations. *Phys. Rev. B* **1977**, *16*, 1746−1747

(44) Methfessel, M.; Paxton, A. T. High-Precision Sampling for Brillouin-Zone Integration in Metals. *Phys. Rev. B* **1989**, *40*, 3616−3621

(45) An, W.; Zeng, X. C.; Turner, C. H. First-Principles Study of Methane Dehydrogenation on a Bimetallic Cu/Ni (111) surface. *J. Chem. Phys*. **2009**, *131*, 174702-1−174702-11.

(46) Kittel, C.; McEuen, P. Introduction to Solid State Physics. Wiley, New York, **1976**.

(47) Sheppard, D.; Xiao, P.; Chemelewski, P.; Johnson, D. D.; Henkelman, G. Generalized Solid-State Nudged Elastic Band Method. *J. Chem. Phys*. **2012**, *136*, 074103-1−074103-08.

(48) Sheppard, D.; Terrell, R.; Henkelman, G. Optimization Methods for Finding Minimum Energy Paths. *J. Chem. Phys*. **2008**, *128*, 134106-1−134106-10.

(49) Henkelman, G.; Jónsson, H. A Dimer Method for Finding Saddle Points on High Dimensional Potential Surfaces Using Only First Derivatives. *J. Chem. Phys*. **1999**, *111*, 7010−7022.

(50) Olsen, R. A; Kroes, G. J.; Henkelman, G.; Jónsson H. Comparison of Methods for Finding Saddle Points without Knowledge of the Final States. *J. Chem. Phys*. **2004**, *121*, 9776−9792.

(51) Wang, S. G.; Cao, D. B.; Li, Y. W.; Wang, J.; Jiao, H. CO_2 Reforming of CH_4 on Ni (111): A Density Functional Theory Calculation. *J. Phys. Chem. B* **2006**, *110*, 9976−9983.

(52) Wang, S. G.; Liao, X. Y.; Hu, J.; Cao, D. B.; Li, Y. W.; Wang, J. Kinetic Aspect of CO_2 Reforming of CH_4 on Ni(111):A Density Functional Theory Calculation. *Surf. Sci*. **2007**, *601*, 1271–1284.

(53) Liu, C.; Ye, J.; Jiang, J.; Pan, Y. Progresses in the preparation of coke resistant Ni-based catalyst for steam and CO_2 reforming of methane. *ChemCatChem* **2011,** *3*, 529-541.

Table 1 Calculated adsorption energies (eV) of the species related to carbon elimination on three types of the alloyed CoNi(111) and the pure Ni(111) surfaces. The energies in bold are the corresponding adsorption energies at the most stable adsorption sites.

Species	Ni(111)		CoNi(111)											
			Model A				Model B						Model C		
	Hcp	Fcc	Hcp1	Hcp2	Fcc1	Fcc2	Hcp1	Hcp3	Hcp4	Fcc1	Fcc3	Fcc4	Hcp	Fcc1	Fcc2
C	**-6.88**	-6.83	**-6.98**	-6.84	-6.83	-6.66	-7.04	**-7.06**	-6.88	-6.88	-6.91	-6.89	**-7.12**	-6.98	-6.97
O	-5.64	**-5.76**	**-5.99**	-5.73	-5.97	-5.74	-5.97	**-6.12**	-5.91	-5.98	-6.09	-5.98	**-6.86**	-6.72	-6.70
OH	-3.35	**-3.45**	-3.64	-3.42	**-3.68**	-3.44	-3.63	**-3.79**	-3.55	-3.65	**-3.79**	-3.69	-3.75	**-3.78**	-3.76
COH	**-4.39**	**-4.39**	**-4.35**	-4.32	-4.10	-4.22	**-4.43**	-4.39	-4.40	-4.40	-4.39	-4.40	**-4.49**	-4.45	-4.43
CO	**-1.89**	-1.87	-1.74	**-1.77**	-1.73	-1.69	**-1.79**	-1.76	-1.76	-1.78	-1.74	-1.76	**-1.82**	-1.78	-1.74
	-1.76[b]	-1.53[a]	-1.70[d]	-1.46[a]	-1.72[c]		-1.48[a]	-1.68[c]					-1.72[c]		

[a] The adsorption energies for CO at the top-Ni; [b] The adsorption energies for CO at the Ni-Ni bridge.

[c] The adsorption energies for CO at the top-Co; [d] The adsorption energies for CO at the Ni-Co bridge.

Table 2 Calculated activation energies (E_a/eV) and reaction energies (ΔH/eV) of C+O and C+OH reactions on the pure Ni(111) and three types of alloyed CoNi(111) surfaces.

Reaction	Paths	Ni(111)		CoNi(111)					
				Model A		Model B		Model C	
		E_a	ΔH	E_a	ΔH	E_a	ΔH	E_a	ΔH
C+O→CO	Path1	2.29	-1.50	**1.52(1.50)***	**-1.13**	**1.50(1.47)**	**-1.04**	**1.36(1.33)**	**-1.02**
	Path2	**1.35(1.33)**	**-1.66**	1.61	-0.94	1.72	-0.77		
	Path3			1.53	-1.12				
	Path4			1.61	-0.93				
	Path5			1.52	-1.10				
	Path6			1.71	-0.92				
C+OH→COH	Path1	1.26	-0.74	**1.19(1.19)**	**-0.52**	**1.32(1.30)**	**-0.44**	1.42	-0.24
	Path2	**1.06(1.04)**	**-0.89**	1.24	-0.50	1.43	-0.23	**1.40(1.38)**	**-0.34**
	Path3							1.41	-0.29

*The values presented in parenthesis are the activation energies with ZPE correction.

Table 3 The rate constant k (s^{-1}) for C+O(OH) reaction at different temperature on the pure Ni(111) and the alloyed CoNi(111) surfaces.

Surface	Reaction	Rate constant k (s^{-1})				
		800K	850K	900K	950K	1000K
Ni(111)	C+O→CO	$9.38x10^4$	$3.15x10^5$	$9.28x10^5$	$2.45x10^6$	$5.87x10^6$
	C+OH→COH	$6.59x10^6$	$1.72x10^7$	$4.06x10^7$	$8.77x10^7$	$1.76x10^8$
Model A	C+O→CO	$8.7x10^3$	$3.38x10^4$	$1.13x10^5$	$3.34x10^5$	$8.89x10^5$
	C+OH→COH	$4.85x10^5$	$1.42x10^6$	$3.72x10^6$	$8.83x10^6$	$1.93x10^7$
Model B	C+O→CO	$2.89x10^4$	$1.1x10^5$	$3.61x10^5$	$1.05x10^6$	$2.75x10^6$
	C+OH→COH	$5.11x10^5$	$1.67x10^6$	$4.78x10^6$	$1.23x10^7$	$2.89x10^7$
Model C	C+O→CO	$1.88x10^5$	$6.36x10^5$	$1.88x10^6$	$4.97x10^6$	$1.2x10^7$
	C+OH→COH	$1.96x10^5$	$6.9x10^5$	$2.11x10^6$	$5.75x10^6$	$1.42x10^7$

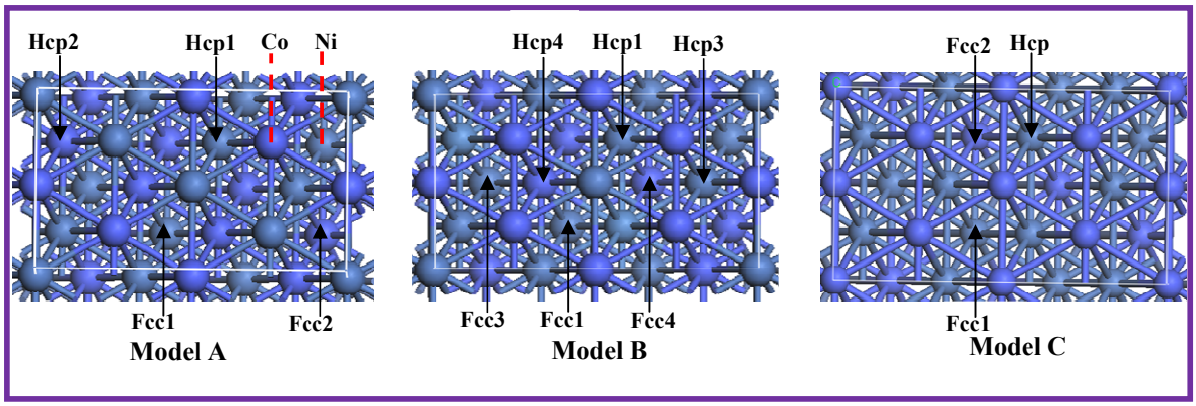

Figure 1 The adsorption sites on Models A~C of CoNi(111) surface. Light sky blue balls stand for Ni atoms, and Neon blue balls stand for Co atoms.

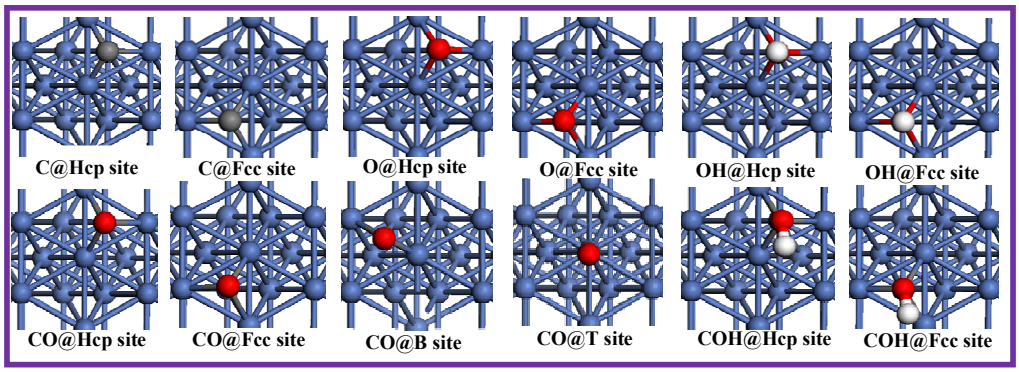

Figure 2 The stable adsorption configurations of the species related to carbon elimination on Ni(111) surface. Grey, white and red balls stand for C, H and O atoms, respectively.

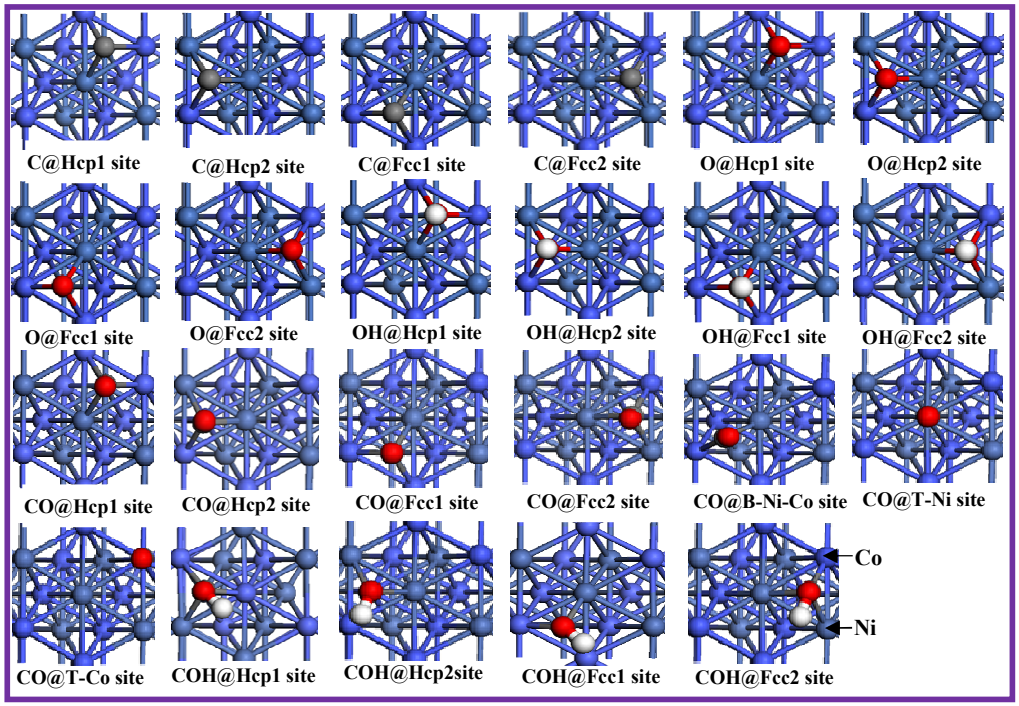

Figure 3 The adsorption configurations of the species related to carbon elimination on Model A of CoNi(111).

See Figures 1 and 2 for color coding.

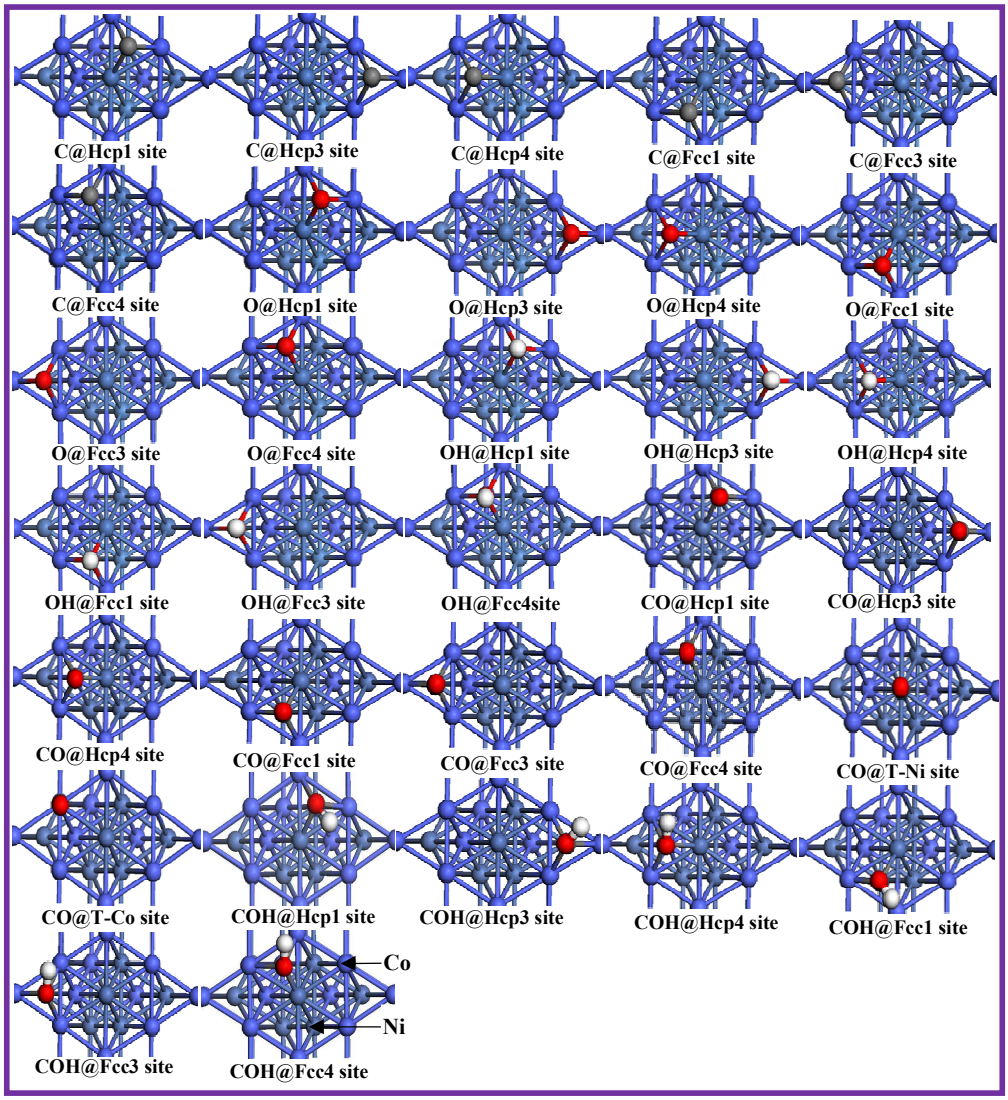

Figure 4 The adsorption configurations of the species related to carbon elimination on Model B of CoNi(111).

See Figures 1 and 2 for color coding.

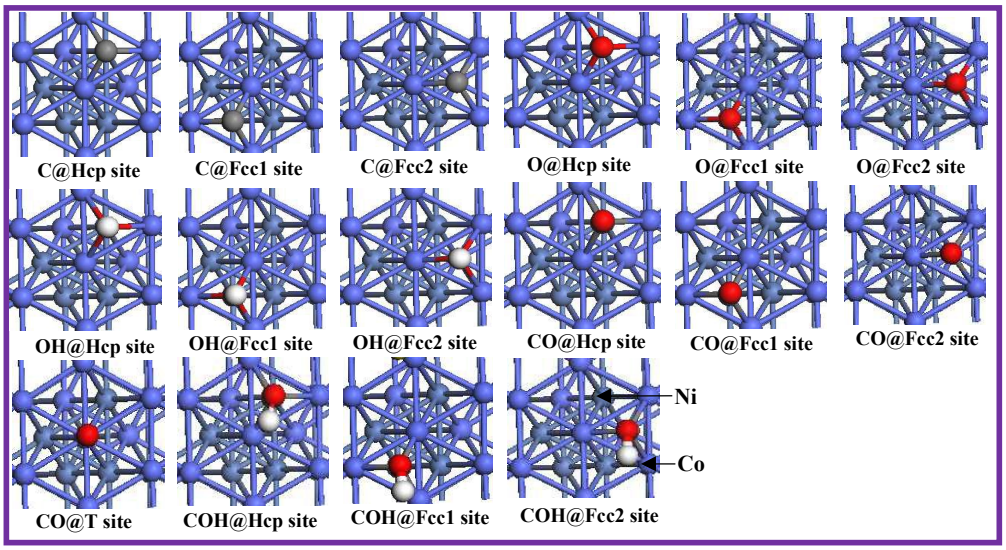

Figure 5 The adsorption configurations of the species related to carbon elimination on Model C of CoNi(111).

See Figures 1 and 2 for color coding.

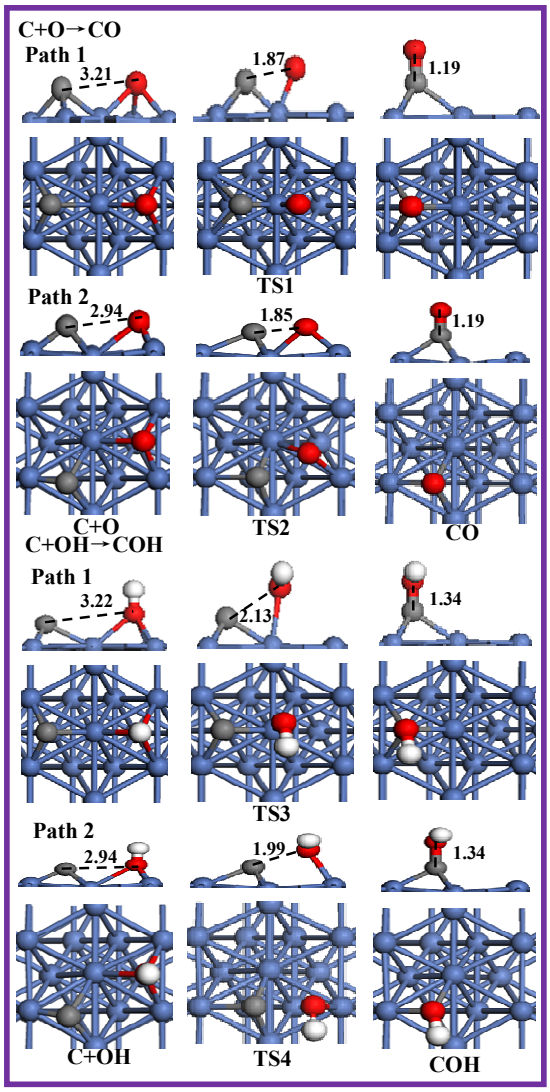

Figure 6 Top views and side views for the structures of the initial states (IS), transition states (TS), and final states (FS) involved in carbon elimination on Ni(111) surface. The unit of bond length is in Å. See Figures 1 and 2 for color coding.

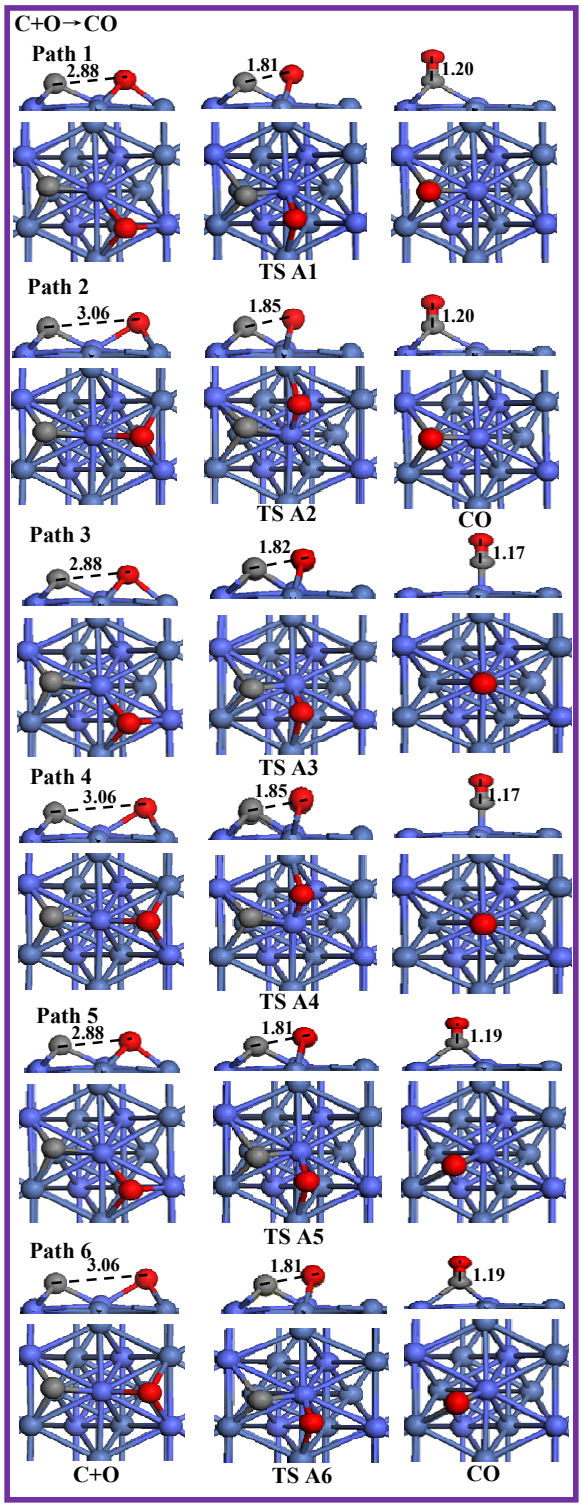

Figure 7 Structures of the stationary states for C+O reaction on Model A of CoNi(111). See Figures 1 and 2 for color coding.

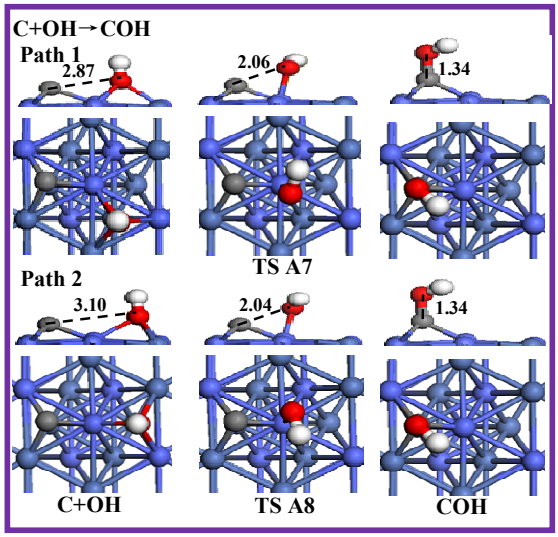

Figure 8 Structures of the stationary states for the association of C+OH on Model A of CoNi(111). See Figures 1 and 2 for color coding.

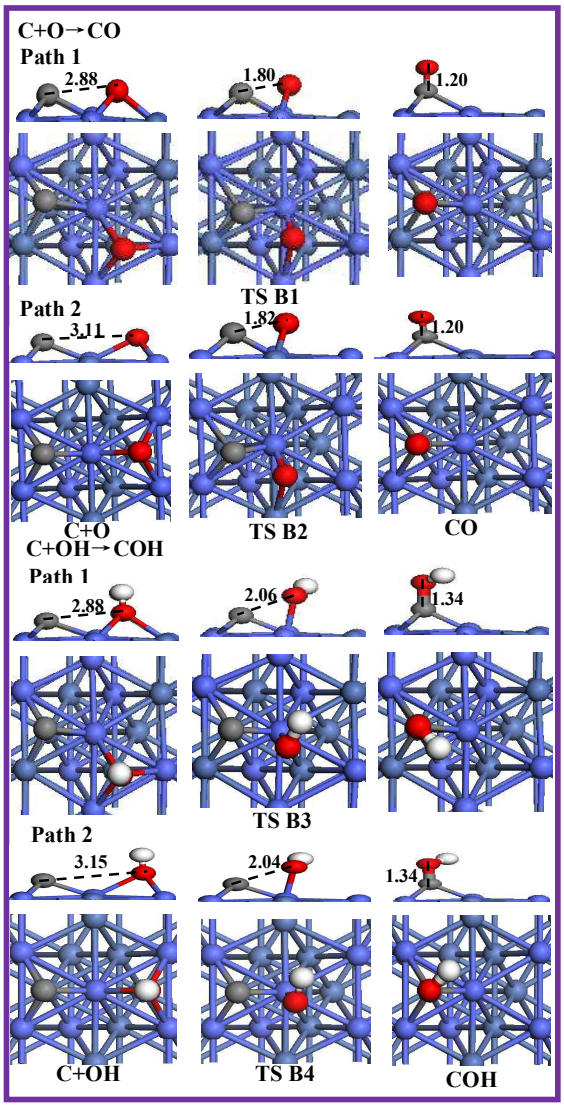

Figure 9 Structures of the stationary states for C+O(OH) reaction on Model B of CoNi(111). See Figures 1 and 2 for color coding.

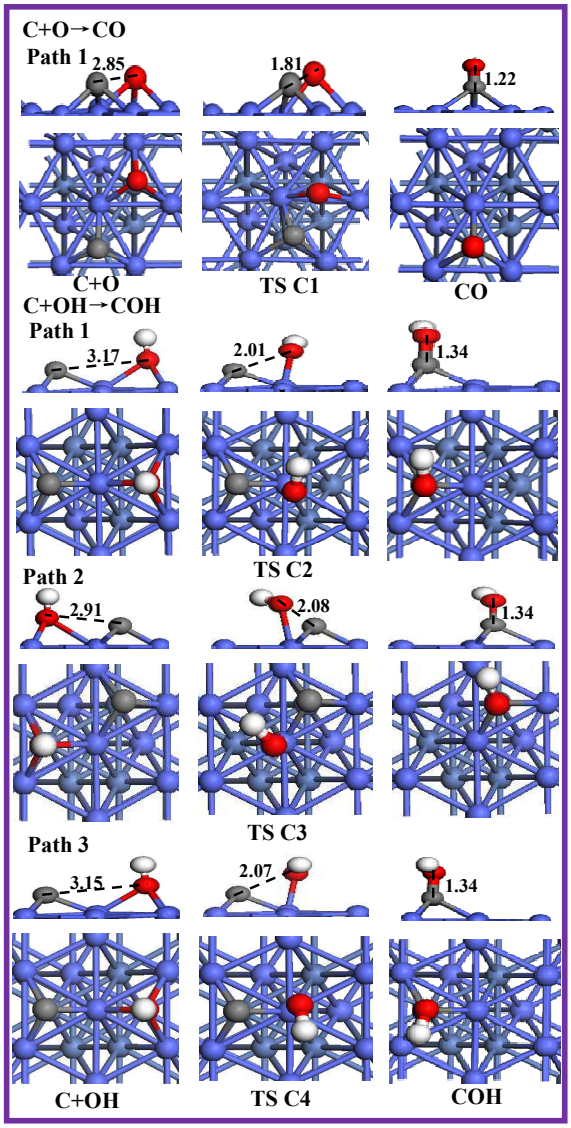

Figure 10 Top views and side views of the structures of stationary states for carbon elimination on Model C of CoNi(111). See Figures 1 and 2 for color coding.